Negative refraction in indefinite media

David R. Smith, Pavel Kolinko, and David Schurig

Department of Physics, University of California, San Diego, 9500 Gilman Drive, La Jolla, Calif. 92093-0319

Manuscript received July 22, 2003; revised manuscript received November 2, 2003; accepted November 12, 2003

Initial experiments on wedge samples composed of isotropic metamaterials with simultaneously negative permittivity and permeability have indicated that electromagnetic radiation can be negatively refracted. In more recently reported experiments [Phys. Rev. Lett. **90**, 1074011 (2003)], indefinite metamaterial samples, for which the permittivity and permeability tensors are negative along only certain of the principal axes of the metamaterial, have also been used to demonstrate negative refraction. We present here a detailed analysis of the refraction and reflection behavior of electromagnetic waves at an interface between an indefinite medium and vacuum. We conclude that certain classes of indefinite media have identical refractive properties as isotropic negative index materials. However, there are limits to this correspondence, and other complicating phenomena may occur when indefinite media are substituted for isotropic negative index materials. We illustrate the results of our analysis with finite-element-based numerical simulations on planar slabs and wedges of negative index and indefinite media.

OCIS codes: 080.0080, 160.1190, 260.2110, 260.1180.

1. INTRODUCTION

When a material possesses simultaneously a negative isotropic permittivity ϵ and a negative isotropic permeability μ, the index of refraction n, as determined by $n = \sqrt{\epsilon}\sqrt{\mu}$, is negative in sign.[1–3] The change in sign of the refractive index has been predicted to lead to a variety of unique electromagnetic phenomena, and materials with simultaneously negative ϵ and μ—frequently referred to as left-handed, negative refractive, or double-negative materials—are currently under scrutiny by the scientific community to explore their various merits.[4]

A fundamental consequence of negative refractive index is the apparent reversal of Snell's law. A wave incident on the interface between two materials whose refractive indices are of opposite sign will emerge from the interface on the same side of the surface normal, rather than on the opposite side. The phenomenon of negative refraction in materials with simultaneously negative ϵ and μ was hypothesized in 1968 by Veselago[4] and was experimentally demonstrated in microwave scattering experiments in 2001.[5] Although various aspects of the experimental results have been questioned,[6,7] negative refraction has nonetheless been confirmed in the most recent set of experiments,[8,9] and its theoretical foundation was further explored.[10–12]

Because no naturally occurring material exists having the property of negative refractive index, experiments to date have been performed on artificially structured metamaterials, for which the negative permeability response results from an array of conducting (nonmagnetic) split ring resonators (SRRs) and the negative permittivity response results from an array of conducting wires. Both the SRR and the wire dimensions are much smaller than the free-space wavelength, so the arrays of scatterers can be approximately described electromagnetically by continuous ϵ and μ tensors.

In the published experiments, *s*-polarized microwaves, in the frequency range of 8–15 GHz, have been used to demonstrate the refractive properties of metamaterials. Given that the fields are restricted to one of the two possible polarizations, the number of relevant material parameter tensor elements is reduced. Applying the coordinates shown in Fig. 1, an *s*-polarized wave will be sensitive only to ϵ_z (the permittivity component in the direction of the applied electric field, polarized along the z axis) and μ_x and μ_y (the permeability components in the plane of propagation). Thus a metamaterial composed of a two-dimensional array of SRRs whose axes are aligned along the x and y directions, with an array of wires oriented along the z direction, can have a negative index of refraction isotropic in the x, y plane for *s*-polarized waves. The experiments presented in Refs. 5 and 9 made use of such a two-dimensional isotropic metamaterial.

Although materials with isotropic negative permittivity and permeability can be described with a negative refractive index, certain classes of anisotropic materials can also exhibit negative refraction.[10–12] We use here the term indefinite medium to refer to a material for which the permittivity and permeability tensor elements (considered along principal axes) are not all the same sign. In the experiment reported by Parazzoli *et al.*,[8] for example, a wedge composed of an indefinite medium formed from SRRs with axes aligned along only one axis (the x axis) and wires oriented along a second axis (the z axis) was used to demonstrate negative refraction. The results indicated no practical difference between the refractive properties of a wedge composed of an isotropic negative index metamaterial (i.e., μ_x, μ_y, and ϵ_z negative) versus those of a wedge composed of an indefinite medium, for which only μ_x and ϵ_z were less than zero.

Because there are nuances associated with anisotropic media, it is our goal here to understand in detail the general nature of reflection and refraction at the interface between an indefinite medium and free space. We are in-

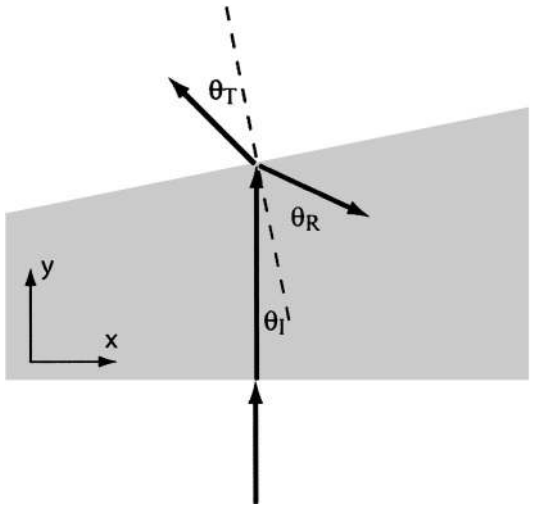

Fig. 1. In a typical negative refraction experiment, a wave from free space impinges on the flat side of a prism sample. The wave passes through the material and undergoes refraction at the second interface as shown. In this diagram, arrows represent the direction of energy flow. In the ensuing analysis, waves are assumed polarized such that the electric field points along the z axis and the magnetic field lies in the plane of propagation (s polarization).

terested in understanding the conditions under which we can substitute an indefinite medium in place of an isotropic negative index medium. We show that, although indefinite media have different dispersion characteristics as compared with isotropic media, they nevertheless display similar, sometimes exact, refractive (both positive and negative) properties as their isotropic counterparts.

2. NEGATIVE REFRACTION IN ANISOTROPIC MEDIA

In a typical Snell's law negative refraction experiment,[5,8,9] a wave is incident normally onto the first interface of a wedge sample, as depicted in Fig. 1. The wave passes into the medium at the first interface, possibly with some reflection but no refraction, propagates through the medium, then undergoes reflection and refraction (into vacuum) at the second interface. Because we allow for the possibility of indefinite media here, we draw the reflected ray at an arbitrary angle θ_R from the surface normal, as the relationship $\theta_R = -\theta_I$ is not generally true for anisotropic media.

Throughout the following discussion, we restrict our attention to the polarization typically used in the experimental research and indicated in Fig. 1. That is, we assume that waves propagate in the x–y plane, with the electric field polarized along the z axis. The behavior of p-polarized waves can be determined trivially by exchanging the components of the permittivity and permeability tensors (μ_z, ϵ_x, and ϵ_y become the relevant parameters). We also assume the external medium to be free space with isotropic $\epsilon = \mu = 1$. To approximate the metamaterial properties, we treat the medium as continuous, having the indefinite permittivity and permeability tensors as follows:

$$\overleftrightarrow{\epsilon} = \begin{bmatrix} 1 & 0 & 0 \\ 0 & 1 & 0 \\ 0 & 0 & \epsilon_{zz} \end{bmatrix} \quad \overleftrightarrow{\mu} = \begin{bmatrix} \mu_{xx} & \mu_{yx} & 0 \\ \mu_{xy} & \mu_{yy} & 0 \\ 0 & 0 & 1 \end{bmatrix}. \tag{1}$$

The permeability tensor in Eq. (1) is not diagonal. However, it is clear from the assumed form of the permittivity that a rotation in the plane can always be performed that will simultaneously diagonalize $\overleftrightarrow{\epsilon}$ and $\overleftrightarrow{\mu}$, so that for our purposes we can generally describe the properties of a medium by specifying the two permeability components in the propagation plane along principal axes and the out-of-plane permittivity component ϵ_{zz}. If the principal axes for the two tensors are not coincident, then specifying the angle of rotation between the two provides a complete description of the medium. Note that we assume $\epsilon_{xx} = \epsilon_{yy} = \mu_{zz} = 1$ always, although any value for these parameters would not alter the results as the s-polarized waves are not sensitive to these components.

Under our assumptions for the wave propagation direction and polarization, Maxwell's equations yield a scalar wave equation for E_z. In free space, the accompanying dispersion relation has the familiar form

$$k_x^2 + k_y^2 = \frac{\omega^2}{c^2}, \tag{2}$$

where k_x and k_y are the x and y components of the propagation vector, ω is the frequency, and c is the speed of light in vacuum. In the medium, for the given polarization, the wave equation yields the dispersion relation

$$\alpha q_x^2 + \beta q_y^2 + \gamma q_x q_y = \frac{\omega^2}{c^2}, \tag{3}$$

where q_x and q_y are the x and y components of the wave vector in the medium and α, β, and γ are given by

$$\alpha = \frac{\mu_{xx}}{\mu_{xx}\mu_{yy} - \mu_{xy}\mu_{yx}} \frac{1}{\epsilon_z},$$

$$\beta = \frac{\mu_{yy}}{\mu_{xx}\mu_{yy} - \mu_{xy}\mu_{yx}} \frac{1}{\epsilon_z},$$

$$\gamma = \frac{\mu_{yx} + \mu_{xy}}{\mu_{xx}\mu_{yy} - \mu_{xy}\mu_{yx}} \frac{1}{\epsilon_z}, \tag{4}$$

where μ_{xy} and μ_{yx} are off-diagonal terms of the permeability tensor. When referring to diagonal $\overleftrightarrow{\epsilon}$ and $\overleftrightarrow{\mu}$ tensors, we denote the components by a single subscript, such as ϵ_x, ϵ_y, and ϵ_z for $\overleftrightarrow{\epsilon}$.

We assume in this section that the interface between free space and the indefinite material lies parallel to the x axis, so that $q_x = k_x$ and k_x can be used to parameterize the solutions. At a fixed frequency, the solutions corresponding to Eqs. (2) and (3) can be depicted as curves (isofrequency curves) on a plot of k_y (and q_y) versus k_x, as shown in Fig. 2.[13]

Isofrequency curves can be used to predict the refractive properties at an interface by a construction such as that shown in Fig. 2. Assuming an outgoing wave vector

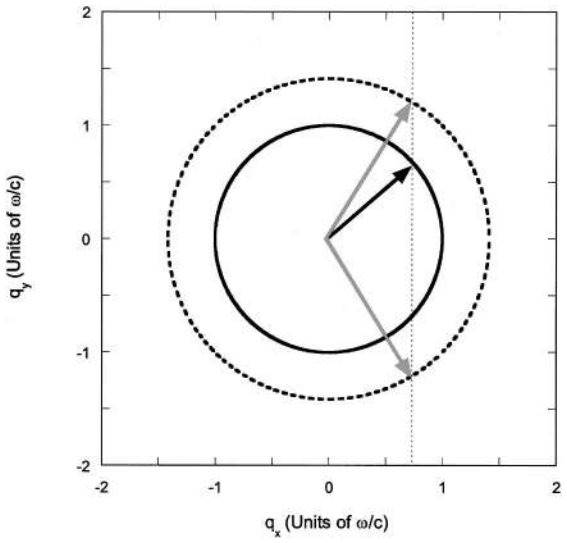

Fig. 2. Isofrequency curves corresponding to free space (solid circle) and an isotropic medium with $|n| = 2$ (dashed circle). Arrows indicate the graphical solution of an interface matching problem, showing both positive and negative refracting solutions.

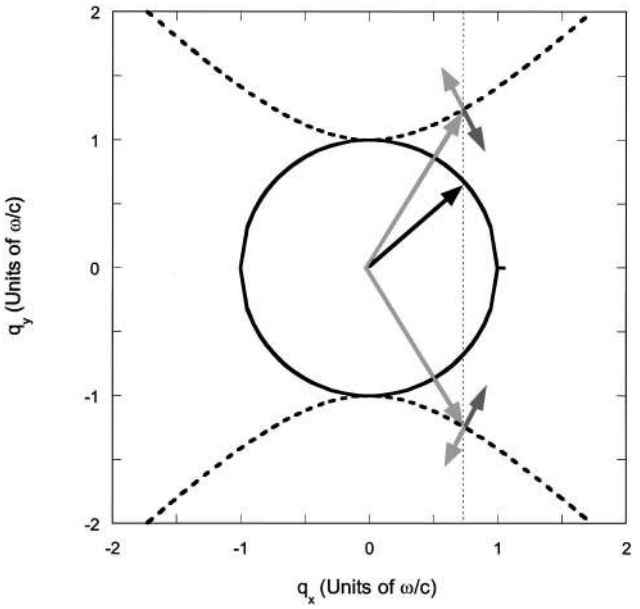

Fig. 3. Isofrequency curves corresponding to free space (solid circle) and an indefinite medium (dashed curves). Arrows indicate the graphical solution of an interface matching problem. The direction of energy flow within the indefinite medium is indicated by the arrows drawn normal to the hyperbolic isofrequency surface. The dark gray arrows indicate the case for negatively refracting indefinite media, and the light gray arrows indicate the case for positively refracting indefinite media.

in free space, indicated by the black arrow, we can find the wave vector solutions in an isotropic medium by noting those points where the parallel (x) component of the wave vector intersects with the isofrequency surface (dashed circle). There are two possible solutions, whose wave vectors are indicated by gray arrows, one corresponding to the incident wave and the other to the reflected wave. The association of a given wave vector with an incoming or outgoing wave, however, depends on the relationship of the direction of the energy flow with respect to the direction of the wave vector. For a medium with negative index, phase and energy velocity are antiparallel, so the solution for a wave in the medium having energy directed toward the interface corresponds to the wave vector directed away from the interface. From this construction, one obtains the result that, at the interface between a positive index material and a negative index material, a wave will undergo negative refraction. Use of isofrequency curves to describe positive and negative refraction has been outlined in Ref. 14.

The isofrequency curves corresponding to indefinite media are distinct from general anisotropic media in that they are characterized by hyperbolic isofrequency curves, as shown in Fig. 3.[14,15] Similar dispersion characteristics can be observed near certain bands in photonic crystals,[16] as well as in anisotropic magnetized plasmas.[17] In these cases, unique wave propagation behavior results.[18]

To determine the refraction behavior of waves incident on an indefinite medium interface, we follow the same process as described for the isotropic medium in Fig. 2. The outgoing wave vector, the black arrow in Fig. 3, now imposes two possible solutions in the medium that correspond to the intersection of the parallel component of the wave vector with the hyperbolic isofrequency curves of the medium. In analogy with positive and negative isotropic media, we define two types of indefinite media having hyperbolic dispersion surfaces: positive and negative refracting. Unlike isotropic media, the energy velocity in indefinite media is neither parallel nor antiparallel to the phase velocity, but rather makes either an acute or an obtuse angle with respect to the phase velocity or wave vector. In general, to distinguish between these two solutions, we must calculate the direction of the Poynting vector with respect to the wave vector for each solution, as we discuss in Section 3. Alternatively, the direction of the energy velocity can be found when we calculate the group velocity, which is generally in the same direction as the energy velocity provided that the frequency is far from regions of anomalous dispersion. The group velocity can be computed from $\mathbf{v}_g = \nabla_{\mathbf{k}}\omega(\mathbf{k})$ and always lies normal to the isofrequency contour.[15] Figure 3 depicts the phase and group-velocity solutions for an interface between free space and an indefinite medium. The permittivity and permeability tensors are assumed to lie along principal axes, with the wave incident at an arbitrary angle to the interface.

The two types of indefinite media with the hyperbolic dispersion surface shown in Fig. 3 can be formed from different combinations of the material parameter tensor elements. A medium for which the signs of ϵ_z and μ_x are less than zero, with μ_y greater than zero, will be negative refracting; for waves propagating in this medium, the angle between the phase and energy velocities of the incident wave will be obtuse. By contrast, a medium for which $\epsilon_z > 0$, $\mu_x > 0$, and $\mu_y < 0$ corresponds to a positive refracting medium; for waves propagating in this medium, the angle between phase and energy velocities will be acute.

3. REFLECTION AND REFRACTION AT AN INDEFINITE MEDIUM INTERFACE

We now solve for the angle of refraction and the reflectance for a wave incident on the interface between free space and an indefinite medium, where the wave is assumed to have the same polarization as described above. A similar study has been performed by Hu and Chui[19] for waves propagating in uniaxially anisotropic indefinite media. Here we present a general analysis that allows for the interface to cut the indefinite material along a nonprincipal axis, leading to the situation depicted in Fig. 4. In general, the incoming and outgoing wave vectors in the medium are no longer necessarily equal in magnitude, nor are their deviations from the surface normal necessarily equal and opposite. The y components of the wave vector can be found by the solution of Eq. (3), which yields

$$q_y = -\frac{\gamma}{2\beta}q_x \pm \left[\left(\frac{\gamma}{2\beta}q_x\right)^2 - \frac{1}{\beta}\left(\alpha q_x{}^2 - \frac{\omega^2}{c^2}\right)\right]^{1/2}. \tag{5}$$

We define $\mathbf{q}_i = q_x\hat{x} + q_y\hat{y}$ and $\mathbf{q}_r = q_x\hat{x} + q_y'\hat{y}$ for the wave vectors corresponding to the wave solutions propagating toward and away from the interface in the medium. Making this distinction, the incident, refracted, and reflected angles can be found from

$$\theta_I = \tan^{-1}\frac{k_x}{q_y},$$

$$\theta_T = \tan^{-1}\frac{k_x}{k_y},$$

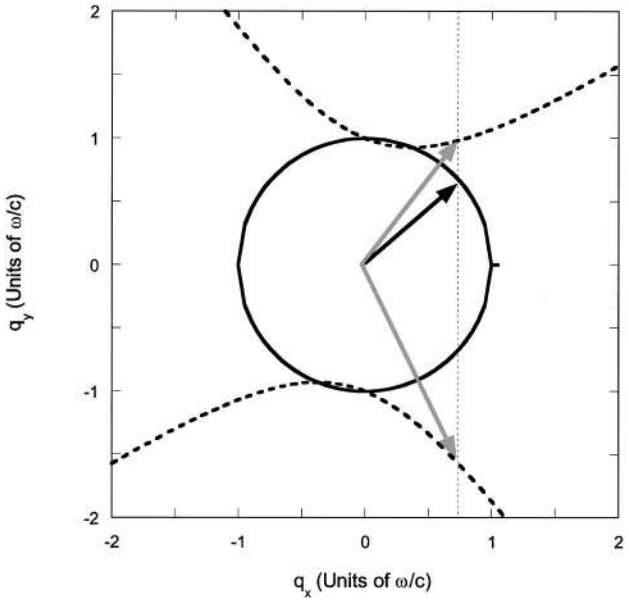

Fig. 4. Isofrequency curves corresponding to free space (solid circle) and an indefinite medium (dashed curves). The interface here is assumed to cut the indefinite medium along a nonprincipal axis. Arrows indicate the graphical solution of the interface matching problem and show that the two wave-vector solutions in the medium do not have the same magnitudes or directions.

$$\theta_R = \tan^{-1}\frac{k_x}{q_y'}. \tag{6}$$

In addition to the refraction of a wave incident at the interface between the vacuum and an indefinite medium, we are also interested in the magnitude of the reflection coefficient, so we must solve the boundary-value problem at the interface. In the medium, the field is composed of the incident and reflected waves, having the form

$$E_I = \exp[i(q_x x + q_y y)] + r\exp[i(q_x x + q_y' y)], \tag{7}$$

where the electric field is polarized along the z direction and the propagation direction is along the y axis. The transmitted field has the form

$$E_T = t\exp[i(k_x x + k_y y)]. \tag{8}$$

Continuity of the electric field at the interface, assumed to intersect the y axis at $y = 0$, yields the equation

$$1 + r = t. \tag{9}$$

A second equation can be found when we require continuity of the transverse component of the **H** field, which we can find from the electric field by use of the Maxwell curl equation combined with the general constitutive relation $\mathbf{B} = \vec{\boldsymbol{\mu}}\mathbf{H}$:

$$\mathbf{H} = -i\frac{c}{\omega}\vec{\boldsymbol{\mu}}^{-1}\nabla \times \mathbf{E}. \tag{10}$$

Equating the x components of the **H** vectors corresponding to the incident, reflected, and transmitted fields, we have

$$\hat{x}\cdot\vec{\boldsymbol{\mu}}^{-1}\cdot\left(\frac{q_y\hat{x} - q_x\hat{y}}{k_y}\right) + r\hat{x}\cdot\vec{\boldsymbol{\mu}}^{-1}\cdot\left(\frac{q_y'\hat{x} - q_x\hat{y}}{k_y}\right) = t. \tag{11}$$

Combining Eq. (11) with Eq. (9), we find the following expression for the reflection coefficient:

$$r = -\frac{1 - \hat{x}\cdot\vec{\boldsymbol{\mu}}^{-1}\cdot\left(\frac{-q_x\hat{x} + q_y\hat{y}}{k_y}\right)}{1 - \hat{x}\cdot\vec{\boldsymbol{\mu}}^{-1}\cdot\left(\frac{-q_x\hat{x} + q_y'\hat{y}}{k_y}\right)}. \tag{12}$$

As described in Section 2, to determine which of the two solutions in the indefinite material corresponds to the incoming or outgoing waves, we calculate the Poynting vector, or $\mathbf{S} = (c/8\pi)\mathbf{E}\times\mathbf{H}^*$. Using Eq. (10) we write

$$\mathbf{S} = -\frac{c^2}{8\pi\omega}\mathbf{E}^*\times[\vec{\boldsymbol{\mu}}^{-1}(\mathbf{q}\times\mathbf{E})]$$

$$= \frac{1}{8\pi}\frac{c^2}{\omega}|\mathbf{E}|^2\hat{z}\times[\vec{\boldsymbol{\mu}}^{-1}(\mathbf{q}\times\hat{z})], \tag{13}$$

which can be further simplified to

$$\mathbf{S} = \frac{\mu_z}{8\pi}\frac{c^2}{\omega}\frac{\vec{\boldsymbol{\mu}}\mathbf{q}}{\det(\vec{\boldsymbol{\mu}})}|\mathbf{E}|^2. \tag{14}$$

The sign of Eq. (14) determines which of the calculated solutions propagates toward the interface and which propagates away from the interface.

4. REFLECTION AND REFRACTION AT A PLANAR INDEFINITE MEDIUM INTERFACE CUT ALONG PRINCIPAL AXES

To be uniform throughout the following analysis, and to be consistent with the specific geometries studied in Sections 6 and 7, we assume that an *s*-polarized wave is incident on the interface between free space and an indefinite material from within the medium. In this section we also assume that the interface cuts the indefinite medium along a principal axis, as depicted in Fig. 5. Before considering an interface with an indefinite medium, we first present the familiar case of reflection and refraction from an interface between free space and an isotropic, positive index material (with $n > 1$) as shown in Fig. 6. Because the wave is incident from the medium side, total internal reflection occurs for angles of incidence larger than a critical angle θ_C, in this case just above 40°. In this example the permeability is isotropic with a value of $\mu = 2$ whereas the permittivity has a value of unity. Note the occurrence of a Brewster's angle just below the critical angle, where the reflectance reaches a value of zero.

Figure 6 also shows the angle of refraction as a function of the incident angle on the right-hand axis. As expected, the angle of refraction sharply approaches 90 deg where the incident angle nears the critical (total internal reflection) angle.

The Brewster's angle usually arises in the context of a *p*-polarized wave reflected from a medium with positive ϵ and $\mu = 1$.[20] Such waves are characterized by the electric field polarized parallel to the plane of incidence. For the case analyzed in Fig. 6, however, the incident wave is *s* polarized (electric field perpendicular to the plane of incidence); the appearance of the Brewster's angle for this polarization is due to the medium having primarily a magnetic response that reverses the roles of *s* and *p* polarization. If we instead compute the reflectance properties of a medium with $\mu = 1$ and $\epsilon = 2$, we recover the usual result (no Brewster's angle) for *s* polarization, shown by the dashed curve in Fig. 6.

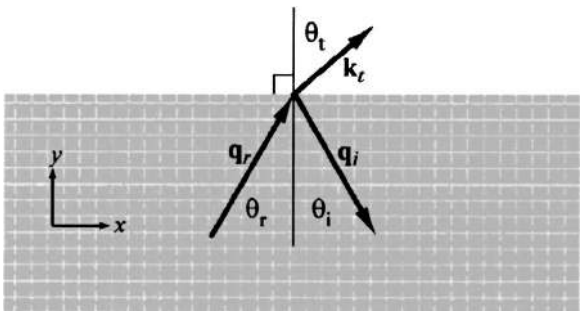

Fig. 5. Shown is a wave, incident from within an indefinite medium, that reflects and refracts from an interface with free space. The principal axes within the medium are indicated by the lighter lines, which show that the interface lies along one of the principal axes. The analysis in Section 4 follows this geometry. Note that even though the phase diagram indicates negative refraction, the group velocity may not in general exhibit negative refraction.

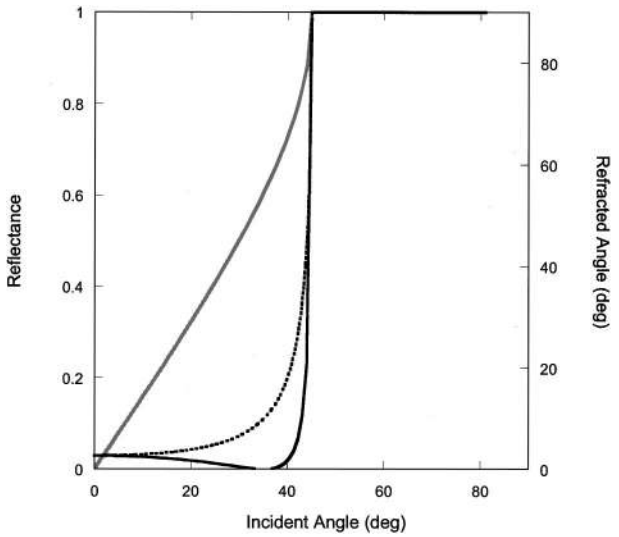

Fig. 6. Reflectance for an isotropic medium with $\mu = 2$ and $\epsilon = 1$ (solid curve) and for an isotropic medium with $\mu = 1$ and $\epsilon = 2$ (dashed curve). The gray curve shows the angle of refraction (right axis).

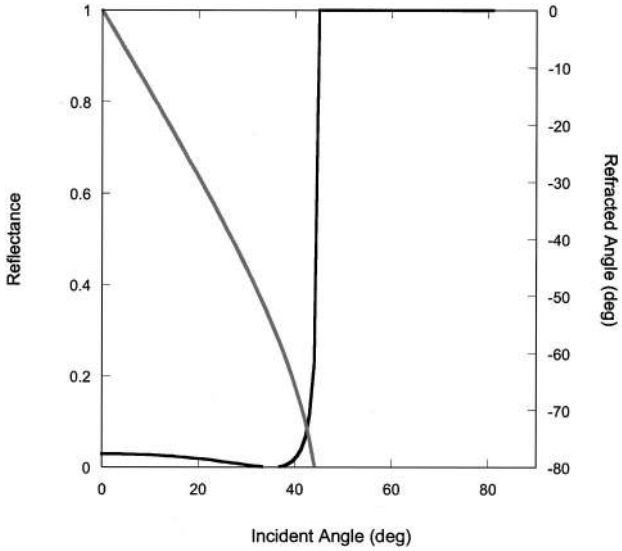

Fig. 7. Reflectance (black curve) and angle of refraction (gray curve) for an isotropic medium with $\mu = -2$ and $\epsilon = -1$. Note that the angle of refraction is for the phase, which is neither parallel nor antiparallel to the direction of energy flow.

The reflection and refraction angles for a wave incident on the planar interface between an isotropic negative index material ($\mu = -2$ and $\epsilon = -1$) and vacuum is shown in Fig. 7. Again, the wave is assumed to be incident on the interface from within the material. The reflectance is identical to that for the positive index case shown in Fig. 6, but the angle of refraction is exactly opposite to that shown in Fig. 6 as the wave is negatively refracted.

As discussed in Section 2 there are two types of indefinite media that exhibit hyperbolic dispersion curves, which we have termed negative and positive refracting. Because we are interested in the type of indefinite medium used in the Snell's law experiments,[8] we consider in

this and in Sections 5–8 only the negative refracting type, for which only ϵ_z and μ_x are negative. For compactness, we describe the material properties of the indefinite medium by specifying the principal axes tensor permeability components $\vec{\mu} = (\mu_x, \mu_y, \mu_z)$ and the z component of its permittivity tensor ϵ_z.

The reflectance and refracted angle for an *s*-polarized wave incident on the interface from within an indefinite medium with permeability $\mu = (-2, 1, 1)$ and $\epsilon_z = -1$ are shown in Fig. 8. Because the interface coincides with a principal axis of the indefinite medium, the angle of reflection of the reflected wave has equal magnitude but opposite sign as the angle of the incident wave. This can be understood from the diagram of Fig. 3, in which the two wave-vector solutions in the medium, represented by the two arrows that intersect the upper and lower hyperbolic curves, have equal magnitude. The indefinite medium appears to behave qualitatively like the isotropic negative index medium shown in Fig. 7, but with the Brewster's and critical angles moved toward a smaller angle. However, the difference is much greater than would at first appear; as the phase and group velocities are not antiparallel in an indefinite medium, we are not able to determine from Fig. 8 the direction of energy propagation of the wave in the medium. In fact, comparison with the isofrequency curves in Fig. 3 shows that the energy is actually positively refracted at the interface. This is the general characteristic of refraction at the interface between free space and a negative refracting indefinite medium cut along a principal axis (parallel to the x axis): Positive group refraction occurs for all incident waves.

The generic reflection and refraction properties of isotropic and anisotropic negative refracting media are similar, as a comparison of Figs. 6–8 shows. However, a negative index medium having isotropic $\epsilon = \mu = -1$ represents a rather unique material condition and deserves further discussion. Such a medium, which has been referred to as antivacuum,[21] has the property that it is perfectly matched to free space. That is, there is no reflection for waves incident on the interface between free space and an $\epsilon = \mu = -1$ medium for any angle of incidence, although there is significant refraction. Remarkable applications have been suggested for matched negative index materials, including subdiffraction imaging[22] and highly efficient, compact low-reflection lenses.[23]

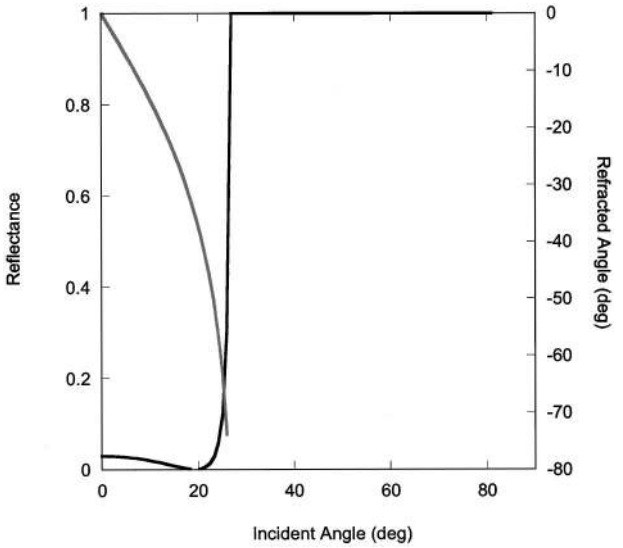

Fig. 8. Reflectance (black curve) and angle of refraction (gray curve) for an indefinite medium with $\mu = (-2, 1, 1)$ and $\epsilon_z = -1$. In this case, the refraction angle for the energy is actually positive.

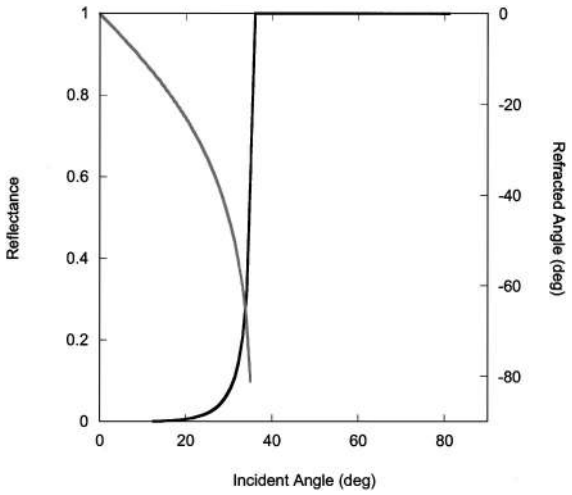

Fig. 9. Reflectance (black curve) and angle of refraction (gray curve) for an indefinite medium with $\mu = (-1, 1, 1)$ and $\epsilon_z = -1$.

Like the isotropic $\epsilon = \mu = -1$ medium, an indefinite medium can also exhibit nearly zero reflectance, but over a restricted range of incident angles. Figure 9 shows the reflectance for waves incident from within an indefinite material characterized by $\mu = (-1, 1, 1)$ and $\epsilon_z = -1$ on a planar interface parallel to the x axis. Over an angular range of approximately 40 deg (20 deg on either side of the normal) the reflectance is close to zero, and the angle of refraction for the wave vector is approximately equal in magnitude (but opposite in sign) to the angle of incidence. If the medium were isotropic with $n = -1$, the reflectance would be zero for all angles, and the refracted angle versus incident angle curve would be linear with a slope of -1.

5. REFRACTION AND REFLECTION AT A PLANAR INTERFACE ALONG NONPRINCIPAL AXES

When the interface does not lie along a principal axis of the permeability tensor, we can apply a straightforward rotation of the tensor to determine the components of the permeability tensor with respect to the new axes defined by the interface. The geometry considered in this section is indicated in Fig. 10. Figure 11 shows three curves corresponding to the diagonal permeability tensor $\mu = (-1, 1, 1)$ and $\epsilon_z = -1$, but with the medium axes rotated by $-10°$, $0°$, and $+10°$ with respect to the interface. As in Section 4, the incident wave is assumed to propagate within the medium, whereas the refracted wave exits the medium into free space. In Fig. 11, the case of $-10°$ is the curve farthest to the left and corresponds to the medium axes as depicted in Fig. 10 being rotated clockwise. The case of the medium axes being rotated $+10°$ is far-

thest to the right in Fig. 10. The qualitative characteristics of refraction and reflection are not significantly altered by the rotation of the principal axes; however, the cutoff angle is shifted.

As the ratio of μ_x/ϵ_z increases from unity, a Brewster's angle emerges and the position of the critical angle also changes. Figure 12 shows the reflectance and the refraction angle as a function of incident angle for values of $\mu_x = -8, -6, -4, -2, -1$, and -0.5, with $\epsilon_z = -1$ always. All other tensor elements have the same values as in Figs. 6–9 and 11, and the medium axes are rotated by $+10°$. For the larger mismatches, the reflectance for normal incidence increases (largest in Fig. 12 for $\mu_x = -8$), and a Brewster's angle is apparent near the incident angle of 20°. When μ_x falls below ϵ_z, however, there is a mismatch at all incident angles, and the Brewster angle vanishes.

Figures 11 and 12 show the refraction and reflection characteristics of waves incident from within a medium, where the direction of propagation of the wave does not necessarily coincide with the principal axis. By contrast, in the experimental wedge geometry one of the principal axes of the indefinite medium typically lies along the first

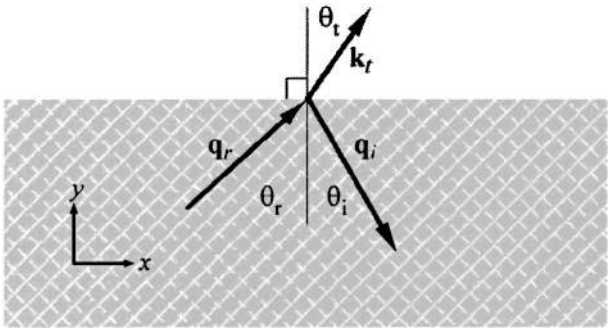

Fig. 10. Shown is a wave, incident from within an indefinite medium, that reflects and refracts from an interface with free space. The principal axes within the medium, depicted by the lighter lines, indicate that the interface does not lie along one of the principal axes. The analysis in Section 5 follows this geometry.

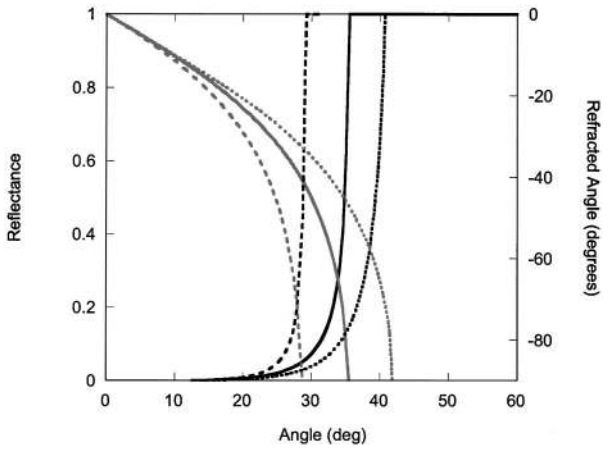

Fig. 11. Reflectance (black curves) and angle of refraction (gray curves) for an indefinite medium with $\mu = (-1, 1, 1)$ and $\epsilon_z = -1$. The principal axes of the medium have been rotated by $-10°$ (leftmost dashed curve), 0° (solid curve), and $+10°$ (rightmost dashed curve). Note that the rotation is with respect to the surface normal, as defined in Fig. 10.

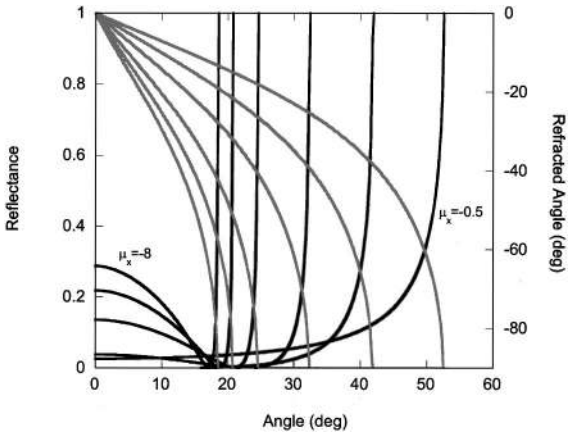

Fig. 12. Reflectance (black curves) and angle of refraction (gray curves) for an indefinite medium with $\mu_x = -8, -6, -4, -2, -1$, and -0.5, with $\epsilon_z = -1$.

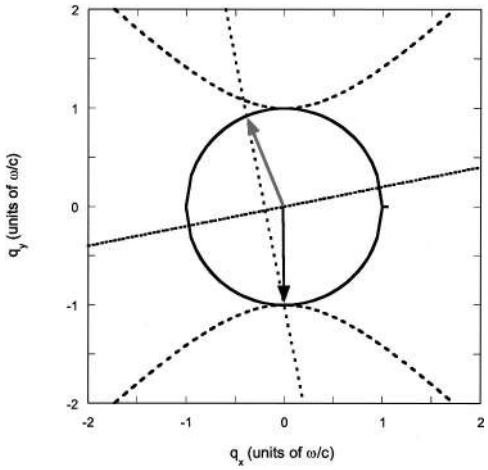

Fig. 13. Isofrequency curves for an indefinite medium (upper and lower dashed curves) and for free space (solid circle). The incident wave is assumed to propagate along the principal axis in the material, for which the phase and group velocities are antiparallel. The black arrow indicates the wave vector corresponding to the indefinite material considered. The short dashed line is plotted along the cut of the interface; a line perpendicular to the interface line and intersecting the tip of the incident wave vector defines the outgoing wave in free space. In this case, the wave undergoes negative refraction at the interface.

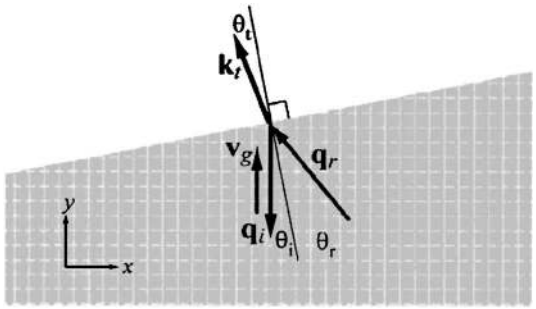

Fig. 14. Negative refracting indefinite medium. The wave vector emerging from the wedge always lies on the same side of the surface normal as the incident wave vector, in the same manner as if the wedge had an isotropic negative index of refraction. The medium parameters are $\mu = (-1, 1, 1)$ with $\epsilon_z = -1$.

interface. Therefore the wave enters the medium and propagates along a principal axis until it reaches the second interface, which does not lie along a principal axis. Although we could pursue the same analysis as above, computing the reflectance and the phase refraction angle, for this geometry it is more instructive to refer to the isofrequency curves, shown in Fig. 13.

For the wave propagating along the principal axis, the phase and group velocities are antiparallel. Thus the incoming wave vector found in Fig. 13 is shown as the black arrow drawn from the origin and intersecting the lower hyperbolic sheet. We assumed in Fig. 13 that the medium is described by $\mu_x = (-1, 1, 1)$ and $\epsilon_z = -1$. Because the wave vector points in the same direction as the phase velocity and is directed away from the interface, the group (or energy) velocity is directed toward the interface. To find the wave vector for the wave refracted into free space, we first draw a line through the origin in the direction of the interface (in this case, 20°). We then draw a second line perpendicular to the interface line that intersects the tip of the incident wave vector; this is equivalently the condition that the component of the wave vector parallel to the interface is conserved. The intersection of this second line with the free-space isofrequency surface determines the outgoing wave vector, in this case indicated by the gray arrow.

The resulting refraction diagram relative to the wedge interface is illustrated in Fig. 14. Figures 13 and 14 show that, for the negative refracting indefinite medium considered ($\epsilon_z < 0$ and $\mu_x < 0$), waves propagating along the principal axis and incident on an interface cut along a nonprincipal axis are always negatively refracted. This behavior is in contrast to the case considered in Section 4, in which waves incident at an angle to an indefinite medium interface cut along principal axes undergo positive group refraction.

Further consideration of Fig. 13 reveals that, so long as the incident wave vector lies along the principal axis of the negative refracting indefinite medium, the refraction properties of an isotropic negative index medium for which $\epsilon = \mu = -1$ and the negative refracting indefinite medium for which $\epsilon_z = \mu_x = -1$ are identical. An indefinite medium can thus be substituted for isotropic negative index media in refraction experiments and potentially other applications, as we discuss in Section 7.

6. SIMULATED REFRACTION FROM INDEFINITE MEDIA WEDGES

In the analysis presented in Section 2, the reflection and refraction properties of an interface are determined by consideration of only three wave excitations: the incident, reflected, and refracted waves. The finite-wedge geometry, however, leads to the possibility of multiple scattering from the two broad interfaces, as well as the sides, of the structure. The additional reflected and refracted waves represent a potential complication to the otherwise simple picture. Because of the unusual reflection and refraction properties of indefinite media, we might expect artifacts related to multiple scattering that may be difficult to predict *a priori*.

To gain some idea of the potential effects due to multiple scattering in the wedge geometry, we can utilize the predicted refraction angles to compute expected ray diagrams for refraction based on geometrical optics. For an indefinite medium with $\mu = (-2, 1, 1)$, we arrive at the diagram shown in Fig. 15 by calculating the angles of reflection at each surface according to the analysis presented above. We assume that the angle of the wedge is 10°. Figure 15 predicts that the incident wave will have a refraction angle of roughly −15° from the surface normal. Although minimal, there is a finite amount of reflectance from the interface such that additional refracted beams are possible. A beam reflected from the bottom surface, for example, would be incident on the interface at an angle of 30° and be refracted at an angle of approximately −60° from the surface normal. A beam reflected from the side would be incident on the wedge interface at

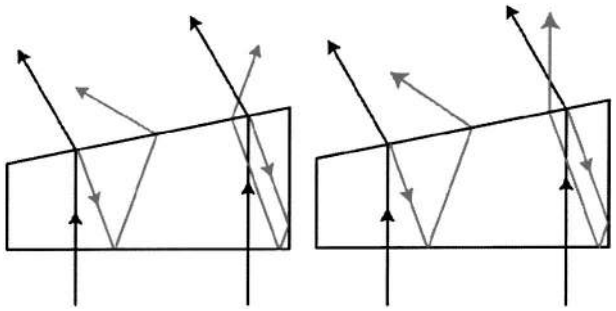

Fig. 15. Ray diagrams showing the possibilities of subsidiary peaks due to multiple reflections in the sample. These ray diagrams take into account the anisotropic properties of the medium, with $\mu = (-2, 1, 1)$ for the wedge on the left and $\mu = (-1.5, 1, 1)$ for the wedge on the right. $\epsilon_z = -1$ in both cases.

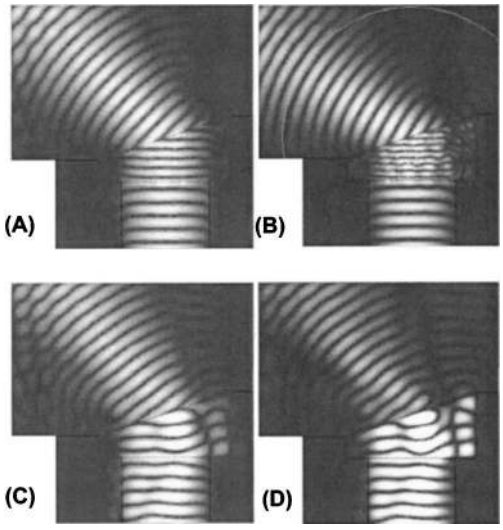

Fig. 16. Numerically computed spatial maps of the magnitude of the electric field for an incident wave refracting from a wedge. The incident wave is guided to the first interface of the wedge by an absorber, for which $\mathrm{Re}(\mu) = \mathrm{Re}(\epsilon) = 1$ and $\mathrm{Im}(\epsilon) = 0.5$. The material parameters of the wedge are (A) $\mu = (-1.4, 1, 1)$ and $\epsilon_{zz} = -1.4$, (B) $\mu = (-2, 1, 1)$ and $\epsilon_{zz} = -2$, (C) $\mu = (-2, 1, 1)$ and $\epsilon_{zz} = -0.5$, (D) $\mu = (-4, 1, 1)$ and $\epsilon_{zz} = -0.25$. In (A) and (B), the index varies but the impedance is matched to free space, whereas in (C) and (D) the index is fixed at $n = 1$, but the impedance varies.

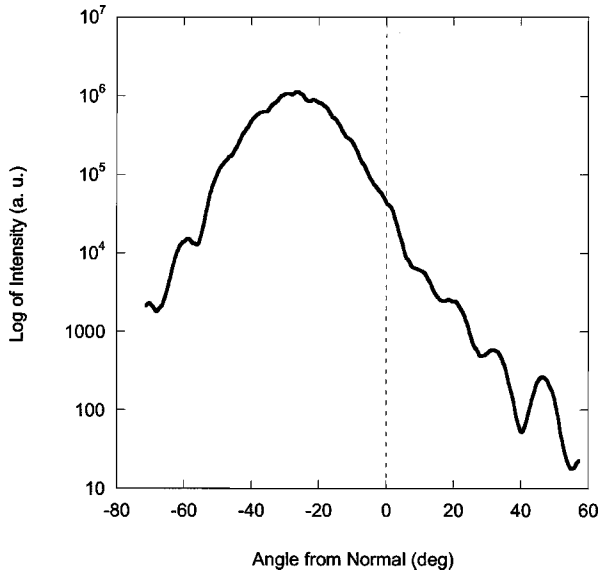

Fig. 17. Angular plot of the log of the field intensity shown in Fig. 16(A), taken along the circumference of the circle depicted in Fig. 16(B). The dashed line corresponds to the angle of the surface normal, defined here as 0°.

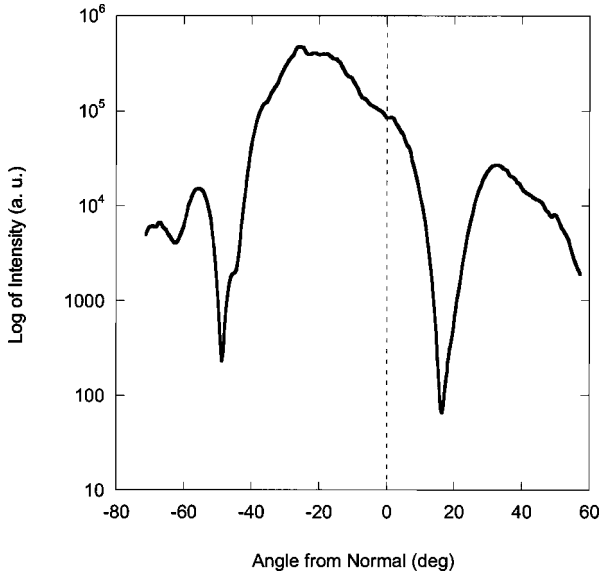

Fig. 18. Angular plot of the log of the field intensity shown in Fig. 16(D), taken along the circumference of the circle shown in Fig. 16(B). The dashed line corresponds to the angle of the surface normal, defined here as 0°.

an angle of −10° and would thus appear to be positively refracted by an angle ~20° from the surface normal. A similar picture is shown on the right in Fig. 15 for a wedge having the parameters $\mu = (-1.5, 1, 1)$. For this sample, the beam reflected from the side wall appears to emerge from the slab in the same direction as the incident beam.

We are thus led to the conclusion that in a refraction experiment in which we use a negative refracting wedge sample, there will likely be two additional refracted beams. One of these beams will refract at an angle more negative with respect to the surface normal than the primary beam, and the other will refract at a positive angle with respect to the surface normal. The relative height of these beams will, of course, depend crucially on the detailed geometry and material parameters. Note that as the mismatch between the indefinite media and the vacuum increases, the possibility for the secondary beams is reduced, as these beams more rapidly encounter total internal reflection.

Because it is nontrivial to determine the refracted fields from a realistic finite-wedge geometry by our analytical methods, we utilize an electromagnetic mode solver to compute the field distributions of waves refracted by finite wedges of indefinite media. The electric field spatial maps shown in Fig. 16 were computed with the driven solution in HFSS (Ansoft). In all examples, only ϵ_z and μ_x of the indefinite media are assumed to be negative and have magnitudes different from unity. Also, the indefinite medium in each of the examples is assumed to be diagonal, with the first interface cut along a principal axis. Thus, if the ratio μ_x/ϵ_z is unity, there will be no reflection from the first surface, but there will generally be reflection from the second wedge interface unless the incident angle providentially corresponds to the Brewster's angle.

The simulated geometry is similar to that used in two-dimensional scattering experiments.[5,8] In these experiments, confining metal plates restrict the polarization of the electric field to lie uniformly along the z direction and further restrict propagation to the x–y plane. An incident aperture is formed by the creation of a channel in absorbing material and with the wedge sample placed directly at the end of the channel. For the simulations, the absorber was modeled by a material for which the real parts of ϵ and μ were equal to unity, with the loss tangent for ϵ_z being 0.05. An incident wave, at a frequency of 10 GHz, was excited at one end of a 10-cm-wide channel in the absorber. The channel extended from where the incident wave was launched up to the first interface of the wedge, which had a length 12 cm.

A spatial map of the magnitude of the field for a wedge with $\mu = (-1.4, 1, 1)$ and $\epsilon_z = -1.4$ is shown in Fig. 16(A). Because $\mu_x/\epsilon_z = 1$, there is no reflection at the first surface and only minimal reflection at the second surface. An angular plot of the field intensity around the circumference of a circle centered on the wedge interface, shown in Fig. 17, thus shows only a single refracted peak. The location of the peak occurs near −25° with respect to the surface normal, as expected for an isotropic sample with an index of $n = -1.4$. Increasing the values of μ_x and ϵ_x, while keeping the ratio μ_x/ϵ_x near unity, leads to similar results, as shown in Fig. 16(B). Note that reflectance begins to increase for nonnormal incidence so that some additional structure exists in the refracted wave for the larger values of μ_x and ϵ_z.

Field plots for the complementary case, wherein the product $|\mu_x\epsilon_z| = 1$, are shown in Figs. 16(C) and 16(D). In Fig. 16(C), $\mu = (-2, 1, 1)$ and $\epsilon_z = -0.5$, so there is a substantial impedance mismatch, even at normal incidence. This increased reflection coefficient can be seen in Fig. 16(C) as the larger field intensity in the absorber channel and throughout the wedge. An even greater mismatch exists for the wedge in Fig. 16(D), for which $\mu = (-4, 1, 1)$ and $\epsilon_z = -0.25$. Note that in both Figs. 16(C) and 16(D) the field structure is within and near the

thicker portion of the wedge (left side of the wedge). Although the ray-tracing picture presented in Fig. 15 is not necessarily an appropriate description, the effect of multiple reflections at the side can clearly be seen and leads to a positively refracted secondary beam. Figure 18 shows the angular plot of the field intensity for the wedge of Fig. 16(D). The primary beam refracts at a somewhat larger angle than the 18° angle of incidence, as expected for an indefinite medium sample with $|\mu_x \epsilon_y| = 1$. However, there are two well-defined secondary peaks, one at a more negative angle than the primary and one positively refracted—consistent with the ray-tracing picture of Fig. 15. Although the secondary peaks are relatively minor in this example (recall that the vertical scale is logarithmic), recent refraction experiments on indefinite media samples indicate secondary beams can be quite substantial.[24]

7. FOCUSING WITH INDEFINITE MEDIA

Our analysis of refraction and reflection at the interface between an indefinite medium and a vacuum indicates that, over a substantial spread of angles, an anisotropic medium can be used in place of an isotropic negative index material. Because the fabrication of three-dimensional isotropic metamaterials can be quite intricate and costly, it is advantageous to use indefinite media samples in experiments to demonstrate phenomena related to negative refraction, as well as in applications that may require negative refracting samples. There are, however, limits to the types of phenomena that can be observed.

An intriguing phenomenon associated with negative refraction that has generated considerable interest is focusing by an isotropic negative index planar slab.[1] The effect is illustrated in Fig. 19(A), which shows the computed spatial map of the electric field produced by a radiating line source next to a finite-width planar slab with $\epsilon = \mu = -1$. The source is a current distribution occupying the area indicated by the circle shown in Fig. 19(A). All fields that emanate from the source and reach the first interface are negatively refracted, effectively reversing their propagation and forming an image within the material. At the second interface, the process is repeated, with the diverging rays from the first image being refocused to the right of the slab. Note that, in principle, the near-field components associated with the source will also be brought to the focus[17]; however, near-field effects are not probed in the calculations presented here.

The spatial Fourier decomposition of a line source is a sum over both homogeneous and inhomogeneous plane waves, with the homogeneous waves emerging in all directions away from the source.[25] Each of these plane-wave components is incident on the first slab interface at some angle to the normal. If the slab is isotropic with $\epsilon = \mu = -1$, then each plane-wave component is negative refracted. In contrast, as was discussed in Section 3, although a slab of negative refracting indefinite media for which $\mu_x = -1$ and $\epsilon_z = -1$ exhibits negative phase refraction, the energy is always positively refracted. This can be seen from Fig. 3, which shows that the group velocity of the refracted wave, indicated on the lower sheet of the hyperbola, is directed into the same quadrant as the incident wave for all angles of incidence. The result is that a line source next to a negative refracting indefinite medium slab does not produce a focus in either the medium or in free space, as shown in Fig. 19(B).

Note that, although the negative refracting indefinite medium planar slab exhibits positive refraction for rays emanating from a diverging source, a positively refracting indefinite medium planar slab will, in fact, exhibit some degree of refocusing. This same mechanism has been previously explored to achieve focusing in certain designs of photonic crystals, which can be effectively modeled with anisotropic permittivity and permeability tensors.[13] Although true aplanatic points are not possible with a planar slab composed of any type of indefinite media, some degree of field enhancement can clearly be obtained, as shown in Fig. 19(C).

The focusing of a source by a planar slab of isotropic negative index material is a unique example of the unusual optics associated with negative refraction and an example of an effect that cannot be reproduced by indefinite media. However, many other lensing or imaging applications enabled by isotropic negative index media can be potentially realized by use of indefinite media, or combinations of different types of indefinite media. A specific example is that of a converging negative index lens. Cited initially as an example of the effect of negative refractive index on geometrical optics, the converging negative index lens was briefly described by Veselago,[1] who noted that a concave negative index lens would have the same function as a convex positive index lens. The comparison between positive and negative index converging lenses was also studied in Ref. 23.

A converging lens formed from an isotropic negative index material having an index $n = -1$ has the same refractive power as a material with an index of $n = +3$, yet can exhibit nearly zero reflection if $\epsilon = \mu = -1$. Figure

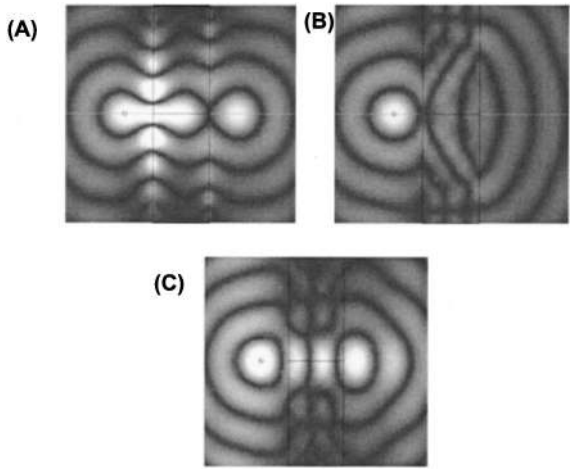

Fig. 19. Line source placed next to (A) an isotropic slab with $\epsilon = -1$ and $\mu = -1$, (B) a slab of negative refracting indefinite media with $\mu_x = -1$ and $\epsilon_z = -1$, (C) a slab of positively refracting indefinite medium with $\mu_z = -1$.

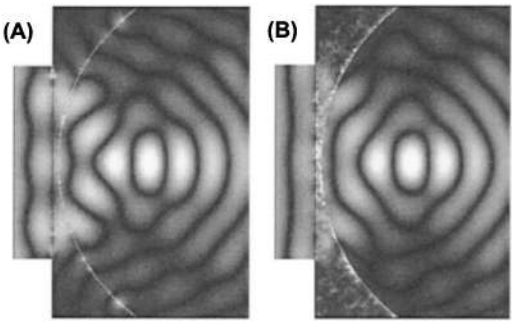

Fig. 20. Spatial map of the computed fields for a converging negative index lens of (A) isotropic material with $\epsilon = \mu = -1$ and (B) indefinite media for which $\mu_x = -1$ and $\epsilon_z = -1$. A plane wave is incident from the left.

20(A) shows the simulated field pattern for an isotropic negative index plano–concave lens ($\epsilon = -1$, $\mu = -1$), driven by a bounded plane wave incident on the flat side. The field at the focus of the lens has been previously shown to be identical to the field pattern at the focus of a positive index ($n = +3$) plano–convex lens.[23]

We expect that we can replace the isotropic negative index material with a negative refracting indefinite material and obtain the same results, because the incident wave propagates within the material uniformly along one axis. As long as the phase and energy directions are antiparallel along this axis, we expect the refraction that occurs on the convex side of the lens to be identical to that which would occur for an isotropic lens, as discussed in Section 4. We thus expect virtually no difference between the isotropic and the anisotropic lenses, as long as the angle of refraction in the indefinite medium is not beyond the cutoff angle. Figure 20(B) confirms the behavior of the indefinite medium lens, which has the identical geometry as the isotropic lens in Fig. 20(A), but with $\mu_x = -1$ and $\epsilon_z = -1$. A comparison of the nodal patterns indicates that the focal properties of the isotropic and indefinite negative refractive lenses are the same. This equivalence, however, is not likely to hold for rays incident at nonnormal incidence.

8. CONCLUSION

In summary, we have performed a detailed analysis of the refraction and reflection characteristics of indefinite media and have shown how these characteristics effect the imaging performance for certain geometries. We conclude that certain types of phenomena may not be possible with indefinite media due to the unique dispersion properties; nonetheless, such applications as converging lenses, with less-strict requirements on numerical aperture, are expected to be feasible. This is an important consideration as the fabrication of higher-dimensional negative refractive metamaterials can be difficult and costly.

ACKNOWLEDGMENTS

We thank Claudio Parazzoli, Kin Li, and Minas Tanielian (Boeing, Phantom Works) for important discussions regarding the experimental aspects of indefinite media. This research was supported by the Defense Advanced Research Projects Agency (DARPA), contract MDA972-01-2-0016. D. R. Smith also acknowledges support from DARPA, contract DAAD19-00-1-0525.

REFERENCES

1. V. G. Veselago, "The electrodynamics of substances with simultaneously negative values of ϵ and μ," Sov. Phys. Usp. **10**, 509–514 (1968).
2. D. R. Smith and N. Kroll, "Negative refractive index in left-handed materials," Phys. Rev. Lett. **85**, 4184–4187 (2000).
3. R. W. Ziolkowski and E. Heyman, "Wave propagation in media having negative permittivity and permeability," Phys. Rev. E **64**, 05662501–05662515 (2001).
4. See the special issue on negative refraction in Opt. Express **11**, (2003), http://www.opticsexpress.org.
5. R. A. Shelby, D. R. Smith, and S. Schultz, "Experimental verification of a negative index of refraction," Science **292**, 79–81 (2001).
6. P. M. Valanju, R. M. Walser, and A. P. Valanju, "Wave refraction in negative-index media: always positive and very inhomogeneous," Phys. Rev. Lett. **88**, 1874011–1874014 (2002).
7. N. Garcia and M. Nieto-Vesperinas, "Is there an experimental verification of a negative index of refraction yet?" Opt. Lett. **27**, 885–887 (2002).
8. C. G. Parazzoli, R. B. Greegor, K. Li, B. E. C. Koltenbah, and M. Tanielian, "Experimental verification and simulation of negative index of refraction using Snell's law," Phys. Rev. Lett. **90**, 1074011–1074014 (2003).
9. A. A. Houck, J. B. Brock, and I. L. Chuang, "Experimental observations of a left-handed material that obeys Snell's law," Phys. Rev. Lett. **90**, 1374011–1374014 (2003).
10. J. Pacheco, Jr., T. M. Grzegorczyk, B.-I. Wu, Y. Zhang, and J. A. Kong, "Power propagation in homogeneous isotropic frequency-dispersive left-handed media," Phys. Rev. Lett. **89**, 2574011–2574014 (2002).
11. S. Foteinopoulou, E. N. Economou, and C. M. Soukoulis, "Refraction in media with a negative refractive index," Phys. Rev. Lett. **90**, 1074021–1074024 (2003).
12. D. R. Smith, D. Schurig, and J. B. Pendry, "Negative refraction of modulated electromagnetic waves," Appl. Phys. Lett. **81**, 2713–2715 (2002).
13. R. A. Silin, "Derivation of refraction and reflection laws by the isofrequency method," Radiotekh. Elektron. (Moscow) **47**, 186–191 (2002) [Translated version: R. A. Silin, J. Commun. Technol. Electron. **47**, 169–174 (2002)].
14. I. V. Lindell, S. A. Tretyakov, K. I. Nikoskinen, and S. Ilvonen, "BW media—media with negative parameters, capable of supporting backward waves," Microwave Opt. Technol. Lett. **31**, 129–133 (2001).
15. D. R. Smith and D. Schurig, "Electromagnetic wave propagation in media with indefinite permittivity and permeability tensors," Phys. Rev. Lett. **90**, 0774051–0774054 (2003).
16. C. Luo, S. G. Johnson, J. D. Joannopoulos, and J. B. Pendry, "All-angle negative refraction without negative effective index," Phys. Rev. B **65**, 2011041–2011044 (2002).
17. R. K. Fisher and R. W. Gould, "Resonance cones in the field pattern of a short antenna in an anisotropic plasma," Phys. Rev. Lett. **22**, 1093–1095 (1969).
18. K. G. Balmain, A. A. E. Luttgen, and P. C. Kremer, "Resonance cone formation, reflection, refraction, and focusing in a planar anisotropic metamaterial," IEEE Antennas Wireless Propag. Lett. **1**, 146–149 (2002).
19. L. Hu and S. T. Chui, "Characteristics of electromagnetic wave propagation in uniaxially anisotropic left-handed materials," Phys. Rev. B **66**, 0851081–0851087 (2002).
20. J. R. Reitz, F. J. Milford, and R. W. Christy, *Foundations of Electromagnetic Theory*, 3rd ed. (Addison-Wesley, Reading, Mass., 1980), pp. 391–394.
21. A. Lakhtakia, "On perfect lenses and nihility," Int. J. Infrared Millim. Waves **23**, 339–343 (2002).

22. J. B. Pendry, "Negative refraction makes a perfect lens," Phys. Rev. Lett. **85**, 3966–3969 (2000).
23. P. Kolinko and D. R. Smith, "Numerical study of electromagnetic waves interacting with negative index materials," Opt. Express **11**, 640–648 (2003), http://www.opticsexpress.org.
24. C. P. Parazzoli and K. Li, Phantom Works, The Boeing Company (personal communication, 2003).
25. W. C. Chew, *Waves and Fields in Inhomogeneous Media* (Institute of Electrical and Electronics Engineers, Piscataway, N.J., 1995), p. 58.